International Journal of Nanomedicine

Dovepress
Taylor & Francis Group

Open Access Full Text Article

ORIGINAL RESEARCH

BPEI-Stabilized Photocatalytic Au/Titania Nanoclusters with Enhanced Antimicrobial Activity for Wound Healing Applications

Junheng Ke[1,2,*], Linhai Jiang[1,3,*], Qi Sun[2], Sifang Wu[2], Houbing Zheng[1,3], Jialin Ye[2], Haisu Zheng[2], Yi Zhong[2], Da Huang[2], Yuanzi Wu[2], Biao Wang[1,3], Zuquan Weng[1,2]

[1]Department of Plastic and Cosmetic Surgery, The First Affiliated Hospital of Fujian Medical University, Fuzhou, Fujian, People's Republic of China; [2]College of Biological Science and Engineering, Fuzhou University, Fuzhou, Fujian, People's Republic of China; [3]Department of Plastic and Cosmetic Surgery, National Regional Medical Center, Binhai Campus of the First Affiliated Hospital, Fujian Medical University, Fuzhou, 350212, People's Republic of China

*These authors contributed equally to this work

Correspondence: Biao Wang; Zuquan Weng, Email 1812166371@qq.com; wengzq@fzu.edu.cn

Introduction: Wound healing requires dressings with bactericidal effects, where photocatalysis utilizes solar energy to generate reactive oxygen species (ROS) for microbial inactivation. However, most photocatalysts depend on non-visible light, hindering solar-driven therapies. This study developed visible light-responsive Au/Titania/BPEI (TAB) nanoclusters embedded in PDMS, offering enhanced stability, antimicrobial efficacy, and resistance-free antibacterial action.

Methods: TAB composites were synthesized as photocatalytic dressings, with Au nanoclusters enhancing visible-light activity. Characterization included XPS, BET, FTIR, XRD, SEM/TEM, and reflectance spectroscopy. Antibacterial performance was evaluated against pathogens under visible light (0–150 mW/cm²) using in vitro (3T3 cytotoxicity) and in vivo murine models, with ROS mechanisms analyzed.

Results: TA composites achieved 80% bacterial inhibition within 30 minutes of visible light exposure, attributed to ROS generation that disrupts bacterial DNA, membranes, and proteins. BPEI integration enhanced photocatalytic stability by reducing Au_x aggregation and sustaining efficacy across light intensities (20–150 mW/cm²) with retained activity (>70% inhibition) even at saturation thresholds. In vivo models demonstrated reduced pro-inflammatory responses and accelerated healing, while 3T3 assays confirmed high biocompatibility (cell viability >90%).

Discussion: This visible light-activated system provides a resistance-free antibacterial alternative to antibiotics and alcohol-based disinfectants. While TA composites effectively address bacterial infections, limitations include residual bacteria (20% survival) and untested efficacy against fungi/viruses. Future work will optimize material performance for near-complete pathogen eradication and integrate biosensors for real-time infection monitoring. The adaptability of our platform to diverse light environments (sunlight to indoor lighting) and ROS-driven mechanism highlights its potential for clinical translation in combating multidrug-resistant infections.

Keywords: photocatalysis, Au nanocluster, titanium dioxide, wound disinfection

Introduction

Wound healing is a highly coordinated process involving a series of biological stages from the initial inflammatory response to the eventual remodeling of the extracellular matrix.[1] However, bacterial infection at the wound site is one of the most common complications, and common species of wound susceptible bacteria have been identified,[2] including *Escherichia coli, Staphylococcus aureus, Acinetobacter baumannii*, and *Pseudomonas aeruginosa*.[3] These wound susceptible bacteria have played a serious hindrance in each stage of wound repair and can even cause serious complications. For example, *E. coli* infection usually causes diarrhea, abdominal pain, and fever, and if the infection spreads, it may also cause complications such as urinary tract infections and bloodstream infections. *S. aureus* infections can lead to blisters, abscesses, and severe infections that can lead to toxic shock syndrome and scalded skin syndrome.[4] The infection of *A. baumannii* and *P. aeruginosa* usually

Received: 5 February 2025
Accepted: 26 July 2025
Published: 12 September 2025

causes local skin redness, swelling, pain and pus secretion, of which *P. aeruginosa* can also cause soft tissue infection, gangrene ecthyma and other problems.[5]

In addition, these bacteria can produce a variety of toxins and enzymes, such as α-hemolysin and coagulase produced by *S. aureus*, and elastase and collagenase produced by *P. aeruginosa*, which can damage host tissues and slow down the healing process. Furthermore, bacterial infection triggers inflammatory responses that attract immune cells to the wound, and while this is the body's natural defense mechanism, excessive inflammation can damage normal tissue and delay healing.

The spread of infection can bring a host of complications in wound management, and thus an early bacteriostatic treatment at the wound site is essential. The clinical use of antibiotics is the primary approaches to treat wound infection.[6] However, the overuse of antibiotics can make bacteria resistant. Moreover, heavy metal ions such as silver ions (Ag^+) have also been widely used in wound treatment, but they are also toxic to the human body due to certain side effects.[7] Therefore, it is urgent to find an antimicrobial method with broad spectrum, limited use of antibiotic, and high safety.

Photocatalytic materials have become a promising alternative for antimicrobial applications due to their ability to produce reactive oxygen species (ROS) under visible light, which can effectively kill a variety of microorganisms.[8] Especially titanium dioxide (TiO_2), Matsunaga et al[9] first reported the use of Pt/TiO_2 to inactivate three microbial cells (*Lactobacillus acidophilus, Saccharomyces cerevisiae* and *E. coli*) through a photochemical process. TiO_2 photocatalytic performance has been extensively studied due to its high catalytic activity, stability, non-toxicity and cost-effectiveness.[10] However, solar-mediated photocatalytic antibacterial still faces challenges, as it is well known that TiO_2 as a photocatalyst can only be mediated under UV irradiation at 4% of the solar spectrum. Therefore, it is urgent to develop photocatalysts driven by visible light.[11]

Common method to improve the catalytic performance of TiO_2 in visible light and expand its application is to introduce heteroenergy levels between TiO_2 band gaps, reduce the band gap energy of nano-TiO_2, and broaden its visible light response range.[12,13] Among the many metallic nanomaterials, gold (Au) has been shown to significantly enhance the photocatalytic efficiency of TiO_2 under visible light irradiation.[14] In the absence of significant surface plasma-resonance, gold nanoclusters (Au_x) can fluoresce in a wide area from visible light to near infrared and has a long lifetime and a large Stokes shift.[15,16] Au_x, with their unique optical properties and biocompatibility, has attracted considerable attention in the field of biomedicine.[17,18] Polydimethylsiloxane (PDMS) is a polymer composed of organosilicon groups. As one of the most promising elastomers, PDMS is low-cost, easy to use, and has good chemical and thermal stability, biocompatibility, corrosion resistance, chemical inertness, and gas permeability.[19–22] Therefore, PDMS has been used in many fields such as thermal devices, sensors, and coatings.[23–30]

In this study, we explored the antimicrobial properties of Au/Titania nanoclusters (TA) composite made of Au_x and TiO_2 under visible light catalysis. For this purpose, we synthesized Au_x and combined it with TiO_2, and enhanced the stability of the catalytic material by adding branched polyethyleneimine (BPEI) to make Au/Titania/BPEI (TAB). A series of in vitro and in vivo experiments were carried out to verify the efficacy of the composite.

Materials and Methods

Materials

The chemicals used for synthesis in this experiment were purchased from Sinopharm Group (Shanghai, China). $HAuCl_4 \cdot 3H_2O$ was purchased from Aladdin (Shanghai, China). L-glutathione (GSH) and TiO_2 were purchased from Sigma Bio (Burlington, MA, USA). Dulbecco's modified eagle medium (DMEM) and fetal bovine serum (FBS) were purchased from Gibco (Waltham, MA, USA). ROS assay dye 2′,7′-dichlorodihydrofluoresceindiacetate (DCFH-DA) was purchased from Beyotime Biotechnology (Shanghai, China). *E. coli, S. aureus, A. baumannii*, and *P. aeruginosa* were purchased from American type culture collection (ATCC, Manassas, VA, USA), and all bacterial strains were cultured in Luria-Bertani (LB) medium (10 g Tryptone, 5 g Yeast Extract, 5 g NaCl) at 37°C using a constant-temperature incubator throughout the experiments.

Synthesis of Au_x

Au_x clusters were synthesized according to a published method with slight modification.[31] In brief, 80 mg of $HAuCl_4 \cdot 3H_2O$ and 92 mg GSH were mixed in 100 mL of deionized water (DI H_2O) at room temperature. The mixture was

stirred to a colorless solution and then heated at 70°C for 24 h through an oil bath. The synthesized product is purified and crystallized by DI H_2O/acetonitrile (1:3, v/v), finally re-dissolved with DI H_2O, and stored in a 4°C refrigerator before use.

Synthesis of TA and TAB Nanocomposites

For TAB nanocomposites preparation, TiO_2 (0.4 g) was dispersed in 200 mL of ethanol by ultrasound, and 4 mL of BPEI solution (86 mg/mL) was added. The mixture was heated in an oil bath at 60°C for 4 h and then cooled to room temperature. BPEI modified TiO_2 (TB) was obtained by centrifugation, washed repeatedly with ethanol and DI H_2O and dried in the air. For both TA and TAB nanocomposites preparation, 100 mL of above as-prepared Au_x aqueous suspension was mixed with 40 mg TiO_2 nanospheres or TB and stirred at room temperature for 5 h. After 10 min at 8000 rpm, TAs and TABs were washed with DI H_2O and dried in vacuum at 80°C overnight.

Characterization of TA and TAB

The X-ray diffraction pattern is obtained by X-ray photoelectron spectrometer (XPS) at 40 kV and 200 mA (ESCALAB 250, ThermoFisher, Waltham, MA, USA). The morphology images of TA/PDMS and TAB/PDMS were taken by scanning electron microscope (SEM, Verios G4, ThermoFisher, Waltham, MA, USA). The material image and energy spectrum (EDS) were characterized by transmission electron microscope (TECNAI G2 F20, ThermoFisher, Waltham, MA, USA). The optical properties of the materials were analyzed by UV-Vis diffuse reflectance spectroscopy (3600I plus,). The materials were measured by X-ray diffraction (XRD, Rigaku Smartlab, Rigaku Corporation, Wilmington, MA, USA). Fourier transform infrared (FTIR) spectroscopy was measured on Nicolet is50 spectrophotometer (ThermoFisher, Waltham, MA, USA). The specific surface area of the materials was measured by specific surface area analyzer (ASAP 2460, Micromeritics, Norcross, GA, USA).

ROS Detection

Five microliters of bacterial suspensions at 1×10^6 colony-forming units (CFU)/mL of *E. coli, S. aureus, A. baumannii*, and *P. aeruginosa* were mixed with 10 mg photocatalyst and 5 mL PBS in A 50 mL quartz tube, respectively. Then, DCFH-DA (10 μM) was added and mixed well. The mixture was then irradiated under 250 W Xe lamp light source (CEL-TCX250, Ceauligth, Beijing, China) with a 420 nm cut-off, and sample was collected every 10 minutes. The fluorescence intensity was detected using a microplate reader (Bio Tek, Synergy H1, USA) with an excitation wavelength of 488 nm and an emission wavelength of 525 nm.

Cytotoxicity Assay

Toxic effects of Au_x, TiO_2, TA and TAB were analyzed using normal 3T3 mouse embryonic fibroblasts (IMMO Biotech, Fuzhou, China). The material extract was obtained by soaking the material in DMEM medium for 24 h. The toxicity of the material PDMS, TA/PDMS and TAB/PDMS was evaluated using 3T3 cells by testing the material extract.

The cells were seeded in a 96-well plate at a density of 1×10^4 cells/well and cultured at 37°C in an 5% CO_2 for 24 h. Then, Au_x, TiO_2, TA, and TAB are added to the medium at final concentrations from 100 to 500 μg/mL. After 24 h of incubation, 100 μL of fresh medium and 10 μL of cell counting kit-8 (CCK-8, Biosharp, Hefei, China) were added to each well, followed by incubation for two hours. The absorbance of each well was measured at a wavelength of 450 nm with a microplate reader (Synergy H1). Relative cell viability was calculated by comparing the absorbance of treated samples and corresponding controls.

Photocatalytic Antibacterial Activity Assays

In the antibacterial experiments, a 250 W Xe lamp with a 420 nm cut-off filter was used as the light source. *E. coli, S. aureus, A. baumannii*, and *P. aeruginosa* were used as model bacteria. One mg of photocatalyst, 5 mL of PBS, and 5 μL of bacterial suspension (1×10^6 CFU/mL) were sequentially added to a 50 mL quartz tube. The suspension was stirred in the dark for 30 minutes to establish adsorption/desorption equilibrium. During the irradiation process, 100 μL of bacterial suspension was taken every 10 min, diluted with PBS to various dilutions, and then 100 μL of the diluted bacterial suspension was cultured on

LB agar plates. After culturing at 37°C for 24 h, the ratio of bacterial colony (in CFU) reduction was calculated as the antibacterial rate.

Animal Experiments

All animal procedures were conducted in strict accordance with protocol No. 2020-SG-001, approved by the Institutional Animal Care and Use Committee at Fuzhou University. The mice were housed in an SPF animal house with a room temperature of 20–25°C and a relative humidity of 40–60%, supplied with conventional irradiated feed and sterilized drinking water. The mice after being placed in the animal house for 7 days were used in the experiment. Thirty male BALB/c mice (20–25 g, 6 weeks old, Wu's Laboratory Animal Company, Fuzhou, China) were randomly divided into 6 groups, blank group, PDMS group, TA/PDMS group, TAB/PDMS group, TA/PDMS + light group, TAB/PDMS + light group, to establish the mouse wound model.

For wound model, after the mice were anesthetized with 4% chloral hydrate, the back hair of the mice was removed with a shaving knife with the help of hair removal cream, and a skin wound with a diameter of 8 mm was made on the back of the mice with a hole punch. On the second day, 1×10^6 CFU/mL of *E. coli, S. aureus, A. baumannii* and *P. aeruginosa* were prepared into a mixed bacterial solution, and the wound of the back of mice was inoculated with 10 μL mixed bacterial solution. The status of wound was observed on the third day, and the wounds of each group of mice were treated with dressings prepared as previously described. The mice in the non-light group were treated without light, the mice in the light group were treated under light, and the treatment time of the light and non-light group was 30 min, and then the operations were repeated once every 3 days. The treated mice were placed on a photographic platform, and the camera was fixed on a bracket 25 cm away from the platform. The wound image of the mice was obtained after the wound was placed in the center of the visual field. The wound area was calculated using ImageJ software.

On the 12th day, for each mouse, a sterile medical cotton swab was gently dipped into the wound exudate, which was placed in sterile liquid medium and cultured at 37°C and 180 rpm for 24 h. Then, the bacterial solution was diluted 4096 times and used for plate coating. After bacteria collection, mice were euthanized by CO_2, and the skin tissue from the wound area was harvested, and the wound tissue was fixed with 4% paraformaldehyde, followed by ethanol dehydration and paraffin embedding. The paraffin-embedded block samples were then sectioned with a microtome to a thickness of approximately 4 μm. The tissue section was rehydrated for hematoxylin and eosin (H & E) staining. HE stained tissue sections were observed by inverted microscope (TC-S-SR, Nikon, Shinagawa-ku, Tokyo).

The wound tissue except the skin was also collected for cytokine quantification. The wound tissue was washed in PBS to remove the blood, then quickly frozen in liquid nitrogen, the tissue is mixed with pre-cooled PBS in a 1:5 (w/v) ratio, and finally fully grounded with a glass homogenizer. The prepared homogenate was then centrifuged at 5000×g for 5 min, and the supernatant was taken for ELISA to detect inflammatory factors. The ELISA experiment was conducted using kits purchased from Beyotime.

Statistical Analysis

Multiple comparisons between the control group and the experimental group were performed by one-way analysis of variance, followed by Dunnett's test. Two independent samples were compared using Student's *t*-test. The data are expressed by mean ± standard deviation, and the experimental data are statistically analyzed using Origin Pro software (version 9.20). $*P < 0.05$, $**P < 0.01$ and $***P < 0.001$ was considered statistically significant for all analyses.

Results

Principle of Photocatalysis of TA Composites

The proposed principle of photocatalysis of TA composite is shown in Figure 1. Due to the unique optical properties of Au_x, it generates electron-hole pairs under visible light irradiation greater than 420 nm, and the photogenerated electron-hole pairs are separated and migrated to the surface of Au_x. Au_x, when adsorbed on TiO_2 transferred electrons to TiO_2, resulting in an energy transition, generating electron-hole pairs, and reduction-oxidation (REDOX) reactions with adsorbed oxygen or water molecules. O_2 dissolved in water would capture electrons to form $\cdot O_2^-$, while h^+ reacted with

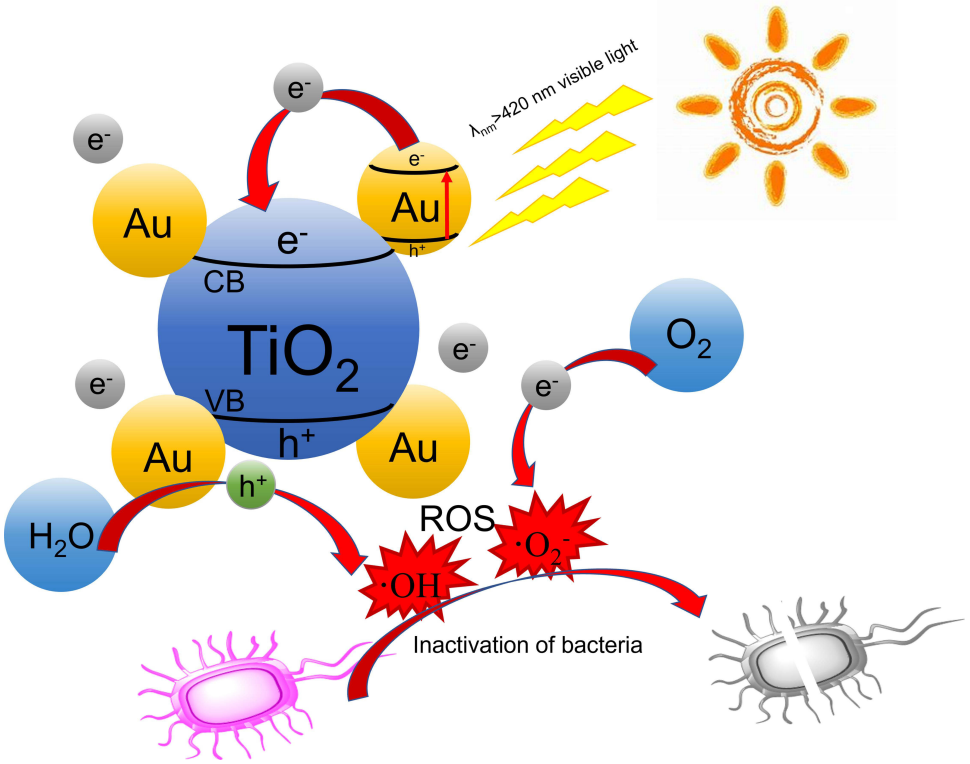

Figure 1 Schematic diagram of the photocatalytic antibacterial principle of composite materials. The unique optical properties of Au_x enable electron-hole pair generation under irradiation above 420 nm. Upon adsorption on TiO_2, Au_x transfers electrons to TiO_2, triggering an energy transition. This mechanism uses TiO_2 to convert water and O_2 into ROS, which inactivate bacteria by inducing DNA damage, membrane rupture, and protein denaturation.

H_2O on the surface to form ·OH. Both $\cdot O_2^-$ and ·OH are recognized as highly reactive oxidizing agents. The presence of ROS upon bacterial cells results in the degradation of cellular DNA, the disruption of cell membranes, and the denaturation of essential proteins, thereby rendering the bacteria inactive. The use of ROS to target bacteria exhibits a broad-spectrum antimicrobial capacity.

Physicochemical Characterization

The morphologies of Au_x and TiO_2, as well as their composite formation, were investigated by TEM and EDX energy spectrum. The morphology of TiO_2, as illustrated in Figure 2A, is characterized by irregular circular shapes with a particle size of approximately 20 nm. The uniform Au_x nanoclusters with an average size of 2.8 ± 0.4 nm (Figure S1) were adsorbed to TiO_2 to form a TA composites, consistent with a previous study.[32] Then, the BPEI modified TiO_2 (TB) was mixed with Au_x solution to obtain TAB. As shown in Figure 2B and C, a substantial quantity of Au_x is observed to be adsorbed onto the surface of TiO_2 within the TA and TAB samples. This conclusion can also be proved by the plane EDX spectra (Figure 2D–F) and point EDX spectra (Figure 2G–I) of TA and TAB. The UV-vis absorption peak of Au_x is about 400 nm.

Next, we studied the Zeta potentials of various composites. Table S1 demonstrates that the synthesized Au_x presents a negative charge of −7.59 ± 0.36 mV, while TiO_2 presents a positive charge of 7.48 ± 0.92 mV, which is consistent with the original theory. Subsequently, we conducted a study on the composition and physical properties of different composite materials. The XPS spectrum (Figure 3A) shows that TA and TAB have characteristic peaks of Au_x specific elements (Au, S and N) compared to TiO_2.

In addition, Figure 3B shows that the two characteristic peaks of TiO_2 in the Ti 2p orbital are 464.40 eV and 458.75 eV. Furthermore, the presence of Au_x imparts varying degrees of blue shift to TA and TAB. Notably, TAB exhibits a more pronounced blue shift compared to TA, attributed to the higher concentration of carbonyl and carboxyl groups in BPEI. It can be seen from Figure 3C that the adsorption of TA and TAB is always greater than the adsorption capacity of TiO_2 when the pressure ratio is greater than 0.8, indicating that the two materials, TA and TAB, have the advantage of being able to

https://doi.org/10.2147/IJN.S520784

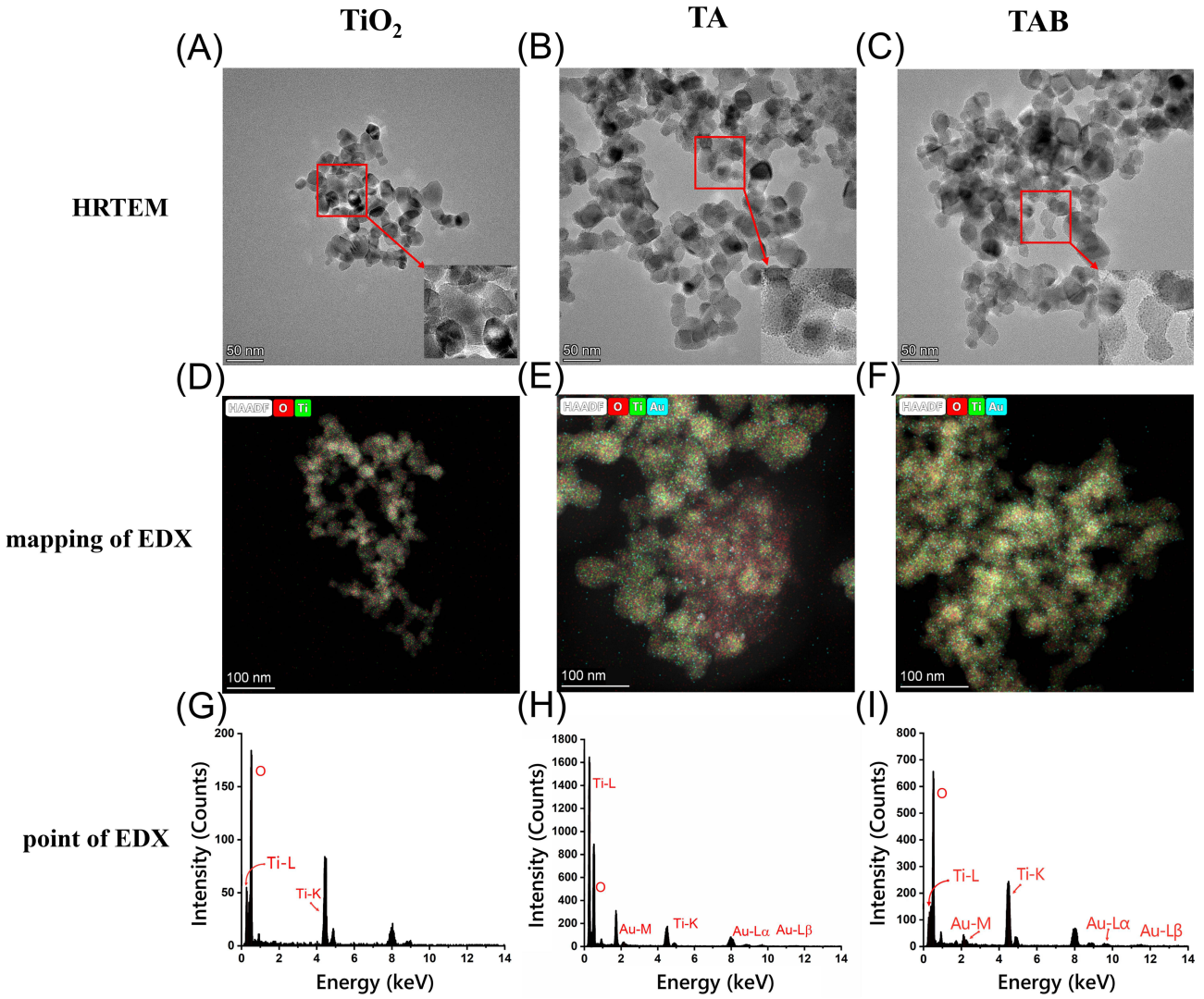

Figure 2 The morphological distribution characteristics of the materials. (**A**–**C**) HRTEM image, (**D**–**F**) mapping of EDX spectrum and (**G**–**I**) point of EDX spectrum of TiO_2, TA and TAB. The neutron diagrams in (**A**–**C**) are enlarged images of the parts in the red box.

photocatalyze under a wider range of wavelengths of light. The FTIR spectrum (Figure 3D) shows that TA and TAB have obvious characteristic peaks around 1500 cm^{-1} but not TiO_2, which is due to the characteristic peaks of Au_x at 1528 and 1588 $cm^{-}1$.[33,34] The XRD pattern (Figure 3E) shows that TA and TAB have the same characteristic peaks as TiO_2, proving the existence of TiO_2. Furthermore, Figure 3F (DRS images) shows that TA and TAB have plasmon resonance peaks at 400–500 nm. The above facts proving the successful synthesis of these composites.

In vitro Antibacterial Activity of TA and TAB Is Related to ROS Produced in Photocatalysis

To evaluate the antibacterial properties of the composites, we evaluated the intracellular levels of ROS in bacteria during photocatalysis (Figure 4). ROS bursts were induced in all bacteria species treated with light-assisted photocatalysis, compared to control or TA or TAB groups, and the production of ROS by TA and TAB escalates in proportion to light time. These results suggest that exposure of TA and TAB to light triggered substantial amount of oxidative stress in all four wound susceptible bacteria.

To assess how light exposure impacts the antibacterial activity of composite materials, we investigated the performance of the composite materials under various lighting conditions. Figure S2 illustrates that sole light irradiation exerts no inhibitory

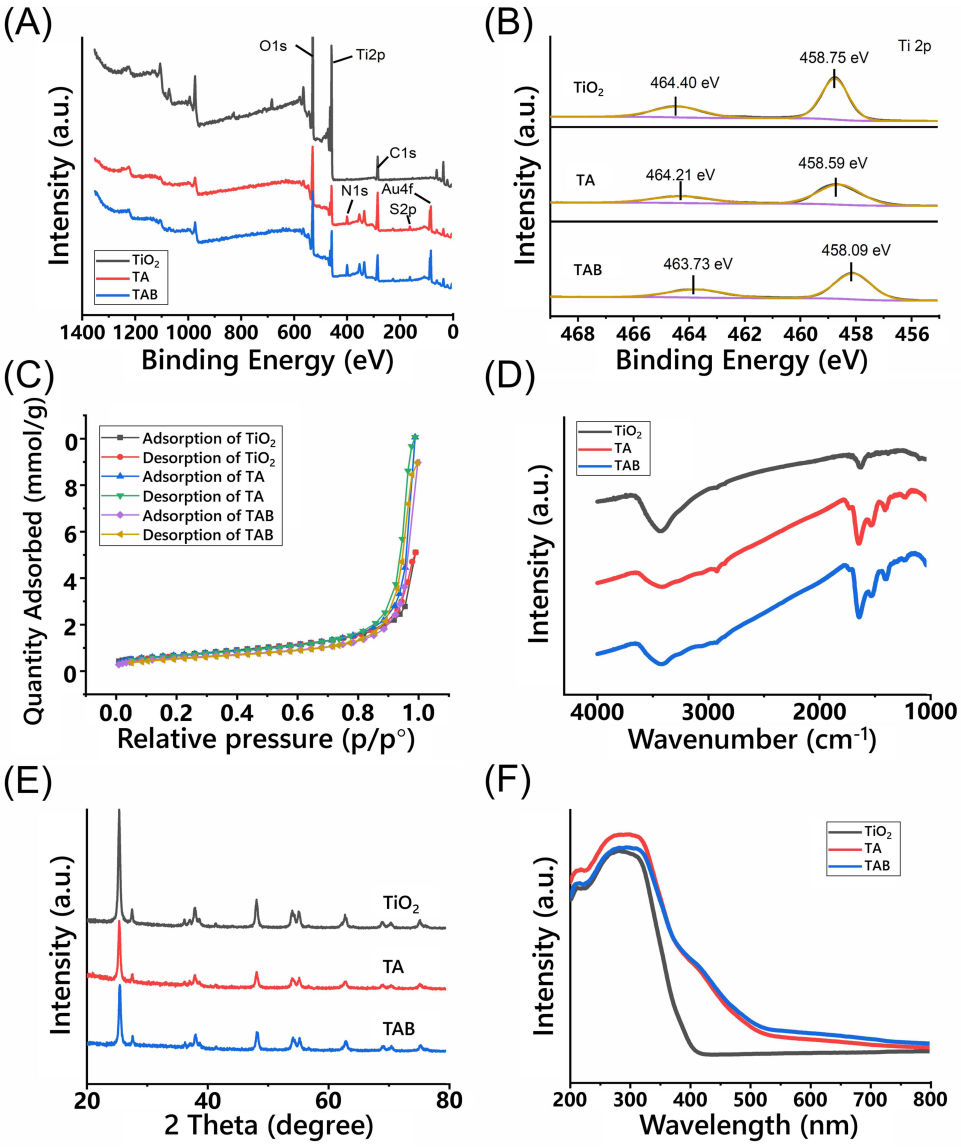

Figure 3 Physical and chemical properties of materials. (**A**) XPS Survey spectra, (**B**) high-resolution Ti 2p spectra, (**C**) Nitrogen adsorption-desorption isotherms, (**D**) FT-IR spectrum, (**E**) XRD patterns and (**F**) DRS patterns of TiO_2, TA and TAB.

influence on *E. coli*, implying that antibacterial efficacy is independent of the lighting per se. Furthermore, a marked divergence from the control group was observed for Au_x in the absence of light, a phenomenon attributed to the ligands around Au_x and its diminutive size. Most importantly, the TA group's antibacterial efficacy under light was markedly enhanced in comparison to both the control group and the TA-only group, indicating that TiO_2 and Au_x only are incapable of eliciting photocatalytic activity under visible light exceeding 420 nm and a pronounced effect is only realized upon their amalgamation.

We further investigated the effects of different photocatalytic conditions on the composites. The photocatalytic antibacterial efficacy is positively correlated with the concentration of photocatalyst (Figure S3), light intensity (Figure S4), ratio of Au_x to TiO_2 (Figure S5), as well as the number of irradiation cycles (Figure S6). Compared with TA, the antibacterial performance of TAB maintains a distinct resilience, retaining approximately 50% of its initial efficacy even after four irradiation cycles. This enhanced durability is attributed to the incorporation of BPEI, which mitigates the aggregation of Au_x particles, consequently augmenting the stability of the photocatalytic process.[35]

The results of photocatalytic antibacterial (Figure 5) show that the antibacterial effect of photocatalysis is also greater with the increase of time, and TAB reached 80% inhibitory effect on 4 common wound susceptible bacteria when the

https://doi.org/10.2147/IJN.S520784

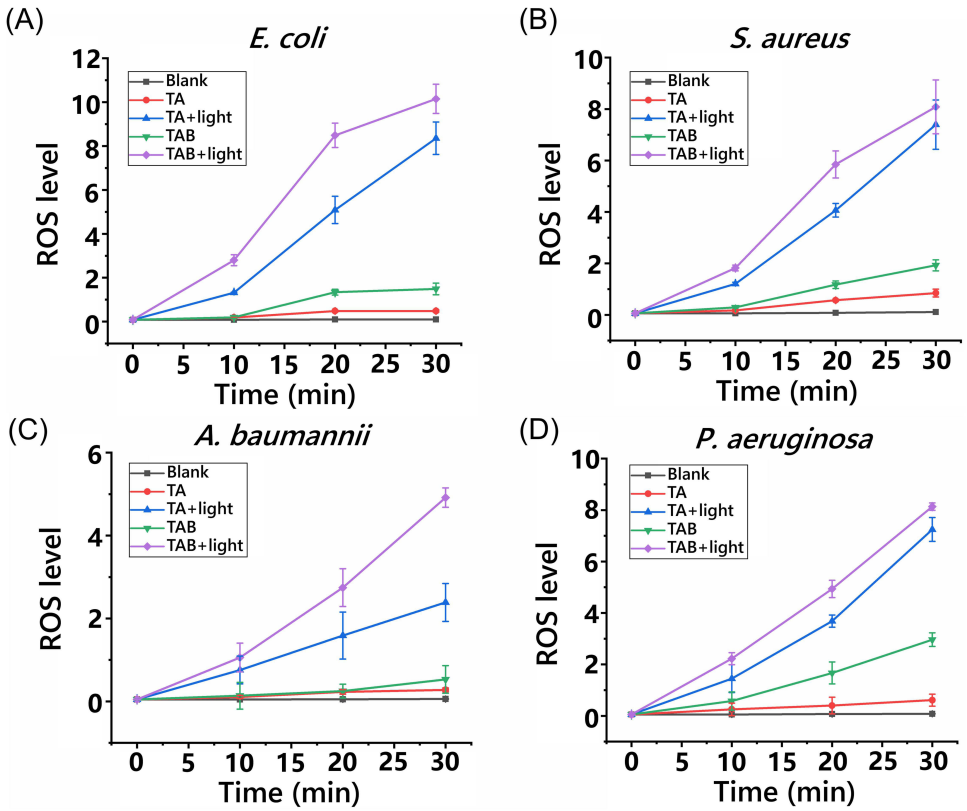

Figure 4 Effect of light exposure time on ROS production in bacteria. When the light intensity is set at 100 mW/cm^2 and the ratio of Au_x to TiO_2 is 0.2, the effect of light exposure time on the (**A**) *E. coli* (**B**) *S. aureus* (**C**) *A. baumannii* (**D**) *P. aeruginosa* is examined under both lighted and non-lighted conditions of the mixed material. (n=5, mean ± SD).

light is lit for 30 min. Notably, the material's antibacterial potency was markedly enhanced when the exposure to light surpassed 20 minutes. This observation also underscores the pivotal role of light in amplifying the material's antibacterial capabilities.

Antibacterial Effect of Dressings in vitro

Prior to investigating the antibacterial efficacy of the dressing, an examination was conducted on how the quantity of photocatalyst present within the dressing influences its antibacterial properties. Figure S7 delineates that an escalation in the photocatalytic antibacterial efficacy is observed concomitant with an increment in the photocatalyst quantity, with the antibacterial potency exhibiting a stabilization trend upon attaining a concentration of 1 mg/mL, which was selected in the subsequent preparation of the dressing.

The antibacterial properties of the dressing were further conducted on murine infection model. Figure S8 illustrates that upon exposure to light, TA/PDMS and TAB/PDMS are capable of eliminating approximately 70% of the four prevalent bacteria typically found in wounds, representing a marked enhancement relative to their respective unexposed counterparts, and the antibacterial efficacy of TAB/PDMS surpasses that of TA/PDMS. However, the addition of PDMS reduced bactericidal potency, which could be attributed to the decrement in the interfacial interaction likelihood between the dressing and the bacterial entities within the aqueous reaction environment.

Evaluation of Biocompatibility

Safety assessment is crucial for biomaterials. Therefore, we further investigated the biocompatibility of the composite material using 3T3 cell line. Figure S9 shows that 3T3 cells maintained a high viability (greater than 80%) when they were treated with Au_x, TiO_2, TA, and TAB at concentration lower than 400 μg/mL. We chose 200 μg/mL, which falls well within the aforementioned safe threshold, for our animal following experiments. Complementary to these findings,

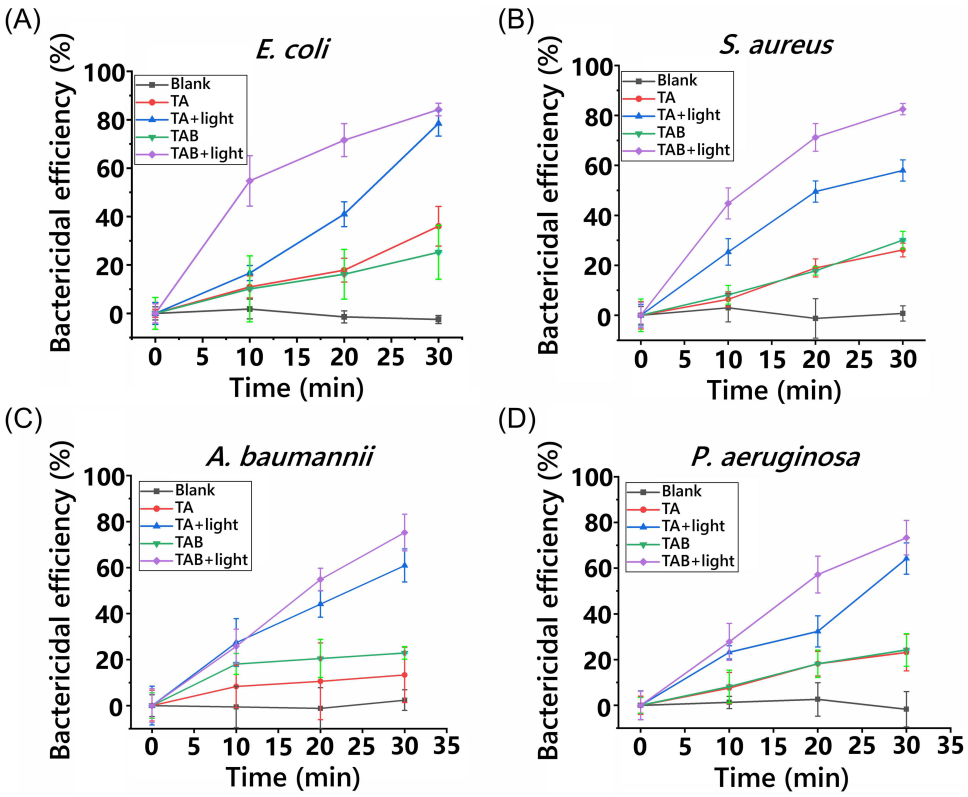

Figure 5 Effect of light exposure time on photocatalytic sterilization. When the light intensity is set at 100 mW/cm^2 and the ratio of Au_x to TiO_2 is 0.2, the influence of light exposure duration on the photocatalytic antibacterial in the (**A**) *E. coli* (**B**) *S. aureus* (**C**) *A. baumannii* (**D**) *P. aeruginosa* is investigated under both lighted and non-lighted conditions of the composite material. (n=5, mean ± SD).

Figure S10 illustrates that cell viability remains above 80% even when exposed to extracts of PDMS, TA/PDMS, and TAB/PDMS at concentrations ranging from 0 to 100 mg/mL for a duration of 24 hours.

Murine Back Wound Experiment

To elucidate the interactions among TA, TAB, and PDMS, we also characterized the planar and cross-sectional structures of TA/PDMS and TAB/PDMS using SEM. As shown in Figure S11A, TA and TAB appeared to overlap on PDMS, forming a rough surface. In addition, it can also be seen from the cross-sectional view of TA/PDMS and TAB/PDMS (Figure S11B) that TA and TAB are stacked and embedded on PDMS.

We further studied the antibacterial properties of the composite in the murine back wound infection model (Figure 6A). The skin wound in mice commenced exudation by the third day (Figure 6B). By the sixth day, a significant reduction in wound exudation was observed in the mice treated with TA/PDMS and TAB/PDMS dressings under light exposure, in comparison to other treatment groups. In addition, on the day 9 and day 12 days, the skin wounds of mice exposed to TA/PDMS and TAB/PDMS dressings and light had gradually healed, which are significantly faster than other treatment groups. The skin wound healing area of the mice using the dressing and lighting reached 80% on the twelfth day (Figure 6C). Mouse skin wound tissue exposed to TA/PDMS and TAB/PDMS dressings and light also possessed a relatively smooth (Figure 6D). Collectively, these findings underscore the feasibility and efficacy of the photocatalytic antibacterial wound dressings in promoting skin wound healing.

Quantification of introduced bacteria at the wound was also performed. Colony plate count showed that, similarly, a marked reduction in bacterial colony formation was observed upon light-assisted dressing group, compared to other groups (Figure 7A). After a quantitative analysis (Figure 7B), it was found that there was only about 20 CFU after using the dressing and light exposure. In contrast, the colony count was about one log higher in the control and non-light groups, demonstrating a pronounced disparity when compared to the group subjected to light. These findings indicate that

https://doi.org/10.2147/IJN.S520784

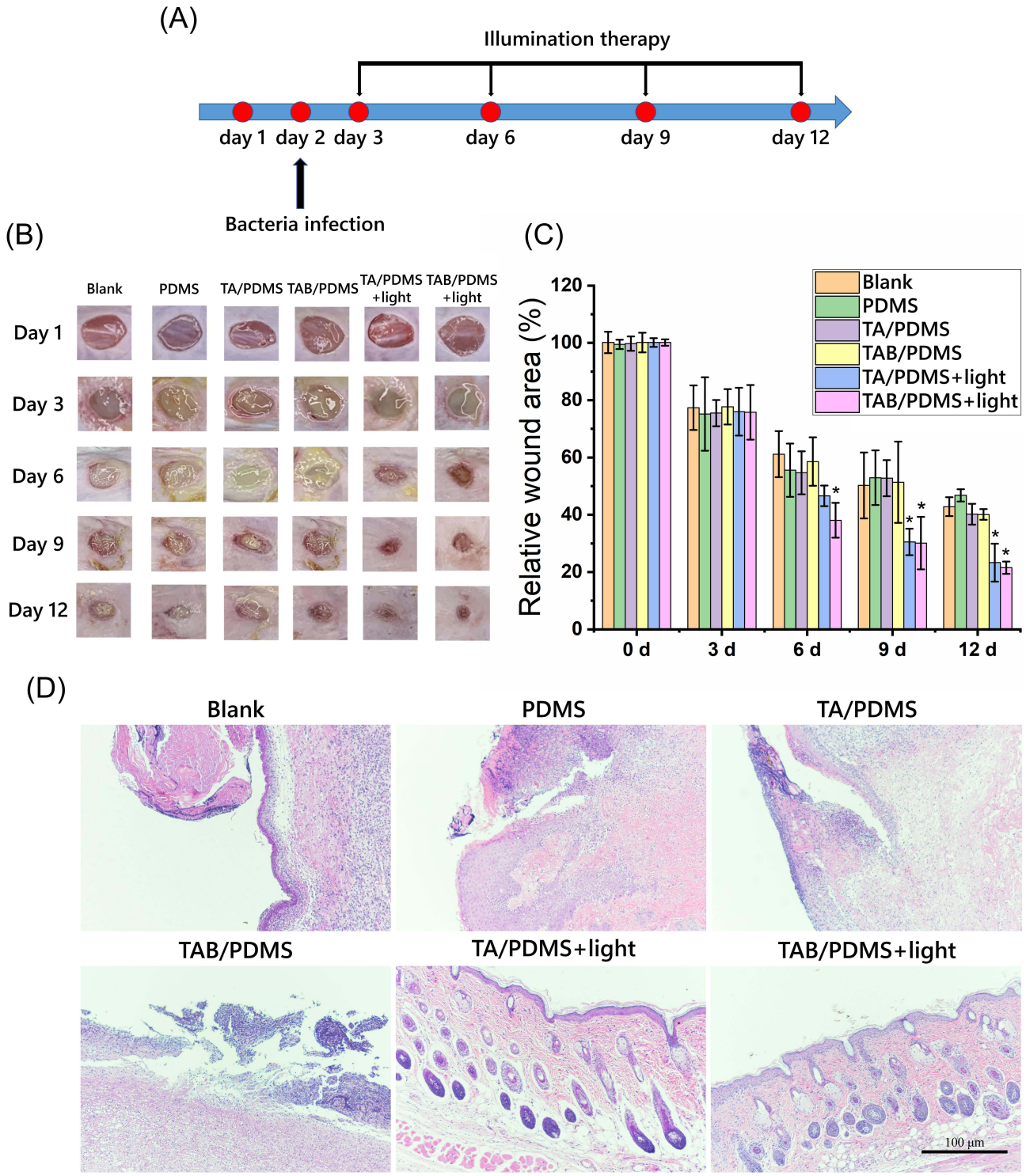

Figure 6 Antibacterial study on wounds on the body's surface. (**A**) Timeline of the animal experiments. (**B**) Representative photos of mouse wounds at different time points. (**C**) Quantitative analysis results of mouse wounds area. (**D**) Photomicrographs showing section of skin tissues with HE staining (40X). *$p < 0.05$, compared to the blank. (n=5, mean ± SD).

the dressing exhibits potent in vitro antibacterial properties and is efficacious in mitigating wound infections on the animal's body surface.

The expression levels of inflammatory cytokines in the wound were also evaluated by ELISA assay. As delineated in Figure 8A–C, the concentrations of interleukin (IL)-6, IL-1β, and tumor necrosis factor (TNF)-α in the wounds treated

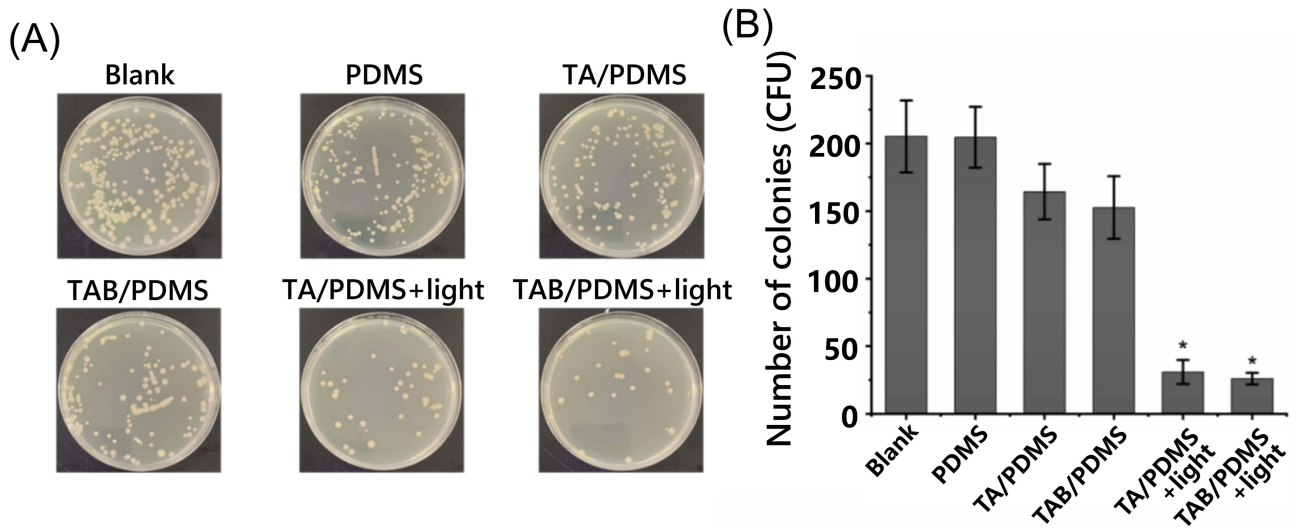

Figure 7 Antibacterial effect of wound dressing in vivo on day 12. (**A**) Plate counting of bacteria in skin wounds, (**B**) Quantitative analysis results of bacteria in skin wounds. *$p < 0.05$, compared to the blank. (n=5, mean ± SD).

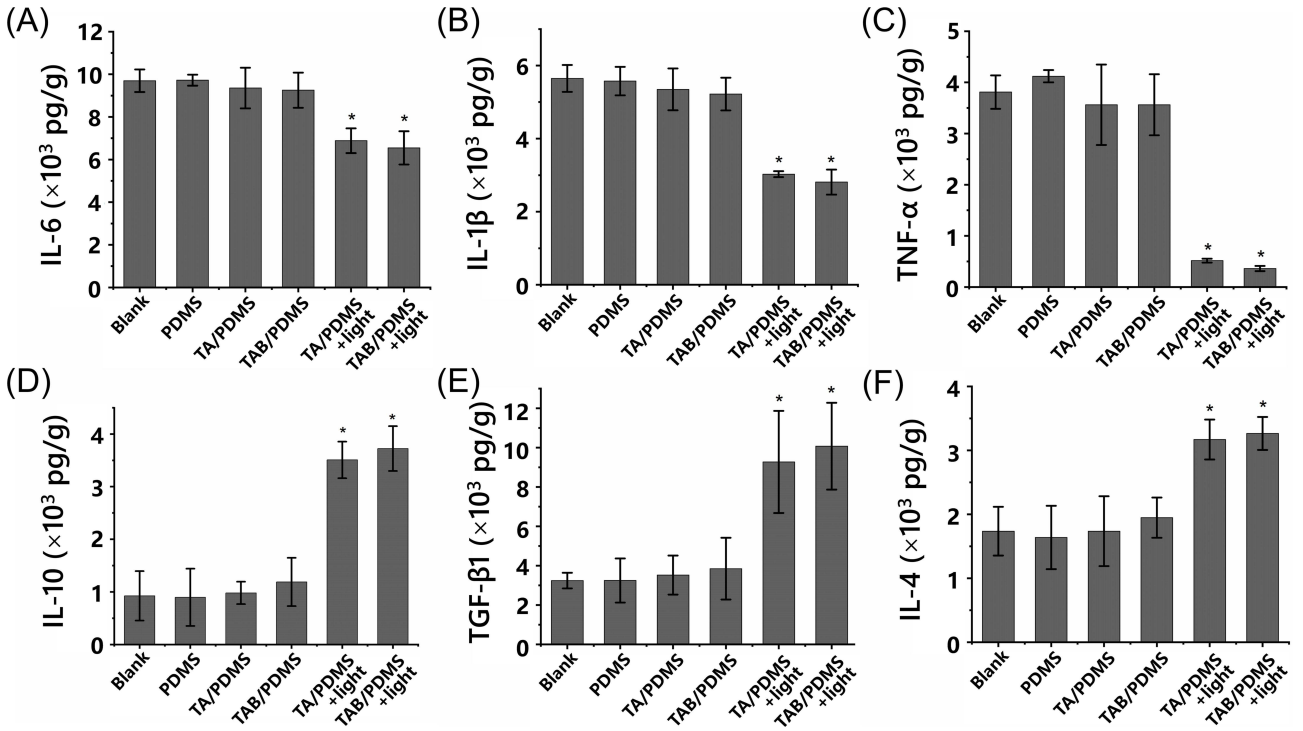

Figure 8 Expression of wound epidermal inflammatory factors and anti-inflammatory factors. The level of (**A**) IL-6, (**B**) IL-1β, (**C**) TNF-α, (**D**) IL-10, (**E**) TGF-β1 and (**F**) IL-4 in the wound. *$p < 0.05$, compared to the blank. (n=5, mean ± SD).

with the dressing and light exposure were markedly reduced compared to those observed in the control group, where significant upregulation of IL-10, transforming growth factor (TGF)-β1, and IL-4 was observed in the wounds treated with the dressing and light exposure. This outcome demonstrates that the photocatalytic antibacterial dressing we engineered is capable of mitigating wound inflammation in murine models while concurrently enhancing the expression of anti-inflammatory mediators, probably through their inherent antibacterial properties.

https://doi.org/10.2147/IJN.S520784

Discussion

Skin injury occurs frequently in daily life, and wound infection can lead to a series of complications, even becoming life-threatening; thus, an effective and prompt anti-bacterial treatment of wound infection is important.

In response to the challenge of bacterial infections in wounds, this study designed TA composite materials, which showed a broad-spectrum antibacterial role through the photocatalysis of visible light irradiation. Meanwhile, reduced pro-inflammatory responses were observed in mouse wound model, which could be attributed to the antibacterial ability of the dressing. Traditional ways such as using aqueous alcohol and isopropanol to wipe the wound area can cause pain, while the misuse or unlimited administration of antibiotics may contribute to appearance of "superbugs". These detrimental microbes gain the ability to evolve and adapt to resistance against traditional antibiotics and can rapidly develop resistance to new drugs,[36] highlighting the importance of developing broad-spectrum antibacterial approaches.

TA composite materials that were utilized in the present study, on the other hand, convert compounds such as water and oxygen into $\cdot O_2^-$ and ·OH in the form of superoxide anions within bacterial cells, causing the damage of cell DNA, the rupture of cell membranes, and the degeneration of key proteins to inactivate bacteria.[37] This method is broad-spectrum and thus does not contribute to drug resistance of bacteria.

In addition, TA composite material we used is a photocatalytic material that can effect under visible light. Our results showed that TiO_2 and Au_x alone cannot produce a photocatalytic effect at visible light greater than 420 nm, and only after their combination, a significant antibacterial effect (~80% of the inhibition rate) can be reached. Although more than 1000 articles on photocatalytic antibacterial have been published in the past two decades,[38] most of the studies failed to achieve antibacterial activity under visible light, endowing our TA composites a broader application range. However, the addition of Au_x did enhance the antibacterial properties of the composite under visible light. However, there is a certain limit for the addition of Au_x, when the ratio of Au_x to TiO_2 reaches 0.2, further increases in the Au_x proportion do not improve the antibacterial efficacy. If the TiO_2 surface adsorb too much Au_x, the gap between Au_x, is the smaller, which makes it easier for the aggregation between Au_x, thus reducing the efficiency of photocatalytic antibacterial.[35] To prevent this, we also added BPEI to reduce the aggregation effect.

When evaluating the effect of light intensity on the composites, the antibacterial effect gradually increased with the increase of light intensity until saturation. However, with the increase of light intensity, the rapid photocatalytic efficiency will lead to the rapid accumulation of Au_x,[35] which eventually reduce the antibacterial effect. Even though the antibacterial effect is reduced under high light intensity, the activity of TA composite materials does not diminish completely and remains at a satisfactory level. This indicates that, whether exposed to direct sunlight with high light intensity or indoor light with low light intensity, TA composite materials can effectively perform their antibacterial function. This enhances their universality in daily applications and minimizes the side effects associated with excessive UV exposure.

Although our TA composites showed good biocompatibility and bioactivity, further work is needed to explore the application limit of their antibacterial properties and to expand their application fields. For example, though our composite could kill 80% of the bacteria after half an hour of light; however, the remaining bacteria, even a small amount, in the wound can still expand and cause inflammation, resulting in serious infections. A further improvement of antibacterial effect of our materials needs to be achieved. Moreover, besides bacteria, fungi and virus are also issues in wound healing. Fungi often obtain nutrients by breaking down skin tissue, which slows wound healing and increases the risk of infection.[39] Viruses usually have less direct effects on skin wounds than bacteria and fungi, but certain viruses, such as herpes simplex virus, can enter the skin through a wound and cause painful herpes or blisters.[40] ROS can inactivate fungal and viral pathogens by oxidizing critical biomolecules: membrane lipids/proteins in fungi, and capsid/envelope components in viruses, while inducing DNA/RNA damage. Therefore, whether the composite material has a sterilization effect on fungi and viruses also needs to be evaluated.

Lastly, we aim to incorporate the embedded biosensors in dressings, allowing them to specifically identify bacteria or bacterial metabolites through antibody-antigen binding or aptamer-based molecular recognition mechanisms, making the killing and inhibition of bacteria more intuitive under our dressing.[41] These approaches help to precisely treat the skin wound site, thereby reducing the risk of wound infection to a greater extent.

Conclusions

In this study, we developed a TiO_2/Au_x-based wound dressing with visible-light photocatalytic antimicrobial activity. By adding BPEI to reduce Au_x aggregation and enhance photocatalytic activity, this dressing inhibits bacterial growth in wounds through generating a substantial amount of ROS under light illumination. The material shows good biocompatibility and excellent antibacterial and associated anti-inflammatory activities and promotes wound healing in a series of in vivo and in vitro experiments. These findings demonstrate the effectiveness of TA composites as antibacterial materials, suggesting their application potential in medical scenarios requiring localized antimicrobial interventions, such as chronic wound care, diabetic ulcer management, or surgical site infection prevention. Future studies should prioritize long-term stability assessments under physiological conditions, scaling protocols for medical-grade manufacturing, and clinical validation of on-demand antibacterial efficacy in human subjects.

Data Sharing Statement

The data generated during the current study are available from the corresponding author on reasonable request.

Funding

This work was supported by Joint Funds for the Innovation of Science and Technology, Fujian Province, China (2021Y9155), and Joint Funds for the Innovation of Science and Technology, Fujian Province, China (2023Y9062), and Joint Funds for the Innovation of Science and Technology, Fujian Province, China (2024Y9169).

Disclosure

There is no conflict of interests regarding the publication of this article.

References

1. Kwiatkowska A, Drabik M, Lipko A, et al. Composite membrane dressings system with metallic nanoparticles as an antibacterial factor in wound healing. *Membranes*. 2022;12(2):215.
2. Nussbaum SR, Carter MJ, Fife CE, et al. An economic evaluation of the impact, cost, and medicare policy implications of chronic nonhealing wounds. *Value health*. 2018;21(1):27–32.
3. Haesler E, Swanson T, Ousey K, Carville K. Clinical indicators of wound infection and biofilm: reaching international consensus. *J wound care*. 2019;28(Sup3b):s4–s12.
4. Wang Z, Feng C, Chang G, Liu H, Zhang WJBID. Enhancing early diagnosis and monitoring of wound infections caused by multiple bacteria in tissues through digital PCR integration with cutaneous infection biomarkers. *BMC Infect Dis*. 2025;25(1):1–10.
5. Ajaba MO, Agbo BE, Umoh N, et al. Investigating the antibacterial potential of thiophene derivatives against wound infections: a combined DFT, molecular docking, and ADMET study targeting Staphylococcus aureus, *Pseudomonas Aeruginosa, and Escherichia Coli Resistant Genes*. *In Silica Pharmacol*. 2024;12(2):111.
6. White RJJOWC. Wound infection-associated pain. *J Wound Care*. 2009;18(6):245–249.
7. Siddiqui AR, Bernstein JMJCID. Chronic wound infection: facts and controversies. *Clin Dermatol*. 2010;28(5):519–526.
8. Bowler PGJAOM. Wound pathophysiology, infection and therapeutic options. *Annal Med*. 2002;34(6):419–427.
9. Matsunaga T, Tomoda R, Nakajima T, Wake HJFML. Photoelectrochemical sterilization of microbial cells by semiconductor powders. *FEMS Microbiol Lett*. 1985;29(1–2):211–214.
10. Shukla SK, Sharma AK, Gupta V, Kalonia A, Shaw PJCDT. Challenges with wound infection models in drug development. *Current drug targets*. 2020;21(13):1301–1312.
11. Bakbolat B, Daulbayev C, Sultanov F, et al. Recent developments of TiO2-based photocatalysis in the hydrogen evolution and photodegradation: a review. *Nanomaterials*. 2020;10(9):1790.
12. Hong Z, Zhang P, He C, et al. Nano-composite of poly (L-lactide) and surface grafted hydroxyapatite: mechanical properties and biocompatibility. *Biomaterials*. 2005;26(32):6296–6304. doi:10.1016/j.biomaterials.2005.04.018
13. Zayats AV, Smolyaninov II, Maradudin AAJPR. Nano-optics of surface plasmon polaritons. *Phys Rep*. 2005;408(3–4):131–314.
14. Yang D, Hassan Q-U, Chen Q-W, et al. Development of novel K0. 8Ni0. 4Ti1. 6O4 nano bamboo leaves, microstructural characterization, double absorption, and photocatalytic removal of organic pollutant. *Environ Res*. 2022;211:113118. doi:10.1016/j.envres.2022.113118
15. Luo Z, Zheng K, Xie J. Engineering ultrasmall water-soluble gold and silver nanoclusters for biomedical applications. *Chem Commun*. 2014;50 (40):5143–5155. doi:10.1039/c3cc47512c
16. Zhang L, Wang E. Metal nanoclusters: new fluorescent probes for sensors and bioimaging. *Nano Today*. 2014;9(1):132–157.
17. Dai D, Liang X, Zhang B, et al. Strain adjustment realizes the photocatalytic overall water splitting on tetragonal zircon BiVO4. *Adv Sci*. 2022;9 (15):2105299. doi:10.1002/advs.202105299
18. Li Y, Yang L, He H, et al. In situ photodeposition of platinum clusters on a covalent organic framework for photocatalytic hydrogen production. *Nat Commun*. 2022;13(1):1355.

19. Van Poll ML, Zhou F, Ramstedt M, Hu L, Huck WTJACIE. A self-assembly approach to chemical micropatterning of poly (dimethylsiloxane). *Angewandte Chemie*. 2007;46(35):6634–6637. doi:10.1002/anie.200702286
20. Berthier E, Young EW, Beebe DJLOAC. Engineers are from PDMS-land, Biologists are from Polystyrenia. *Lab on a Chip*. 2012;12(7):1224–1237.
21. Kuddannaya S, Bao J, Zhang Y. interfaces, Enhanced in vitro biocompatibility of chemically modified poly (dimethylsiloxane) surfaces for stable adhesion and long-term investigation of brain cerebral cortex cells. *ACS Appl Mat Interfaces*. 2015;7(45):25529–25538. doi:10.1021/acsami.5b09032
22. Lee S, Shin H-J, Yoon S-M, Yi DK, Choi J-Y, Paik UJJOMC. Refractive index engineering of transparent ZrO 2–polydimethylsiloxane nanocomposites. *Clin Calcium*. 2008;18(15):1751–1755.
23. Dardouri M, Bettencourt A, Martin V, et al. Using plasma-mediated covalent functionalization of rhamnolipids on polydimethylsiloxane towards the antimicrobial improvement of catheter surfaces. *Biomat Adv*. 2022;134:112563. doi:10.1016/j.msec.2021.112563
24. Kumar R, Sahani AK. Role of superhydrophobic coatings in biomedical applications. *Mat Today*. 2021;45:5655–5659.
25. Bozukova D, Pagnoulle C, Jérôme R, Jérôme C. Polymers in modern ophthalmic implants—Historical background and recent advances. *Mat Sci Eng*. 2010;69(6):63–83.
26. Yu H, Zhou G, Sinha SK, Chau FS, Wang SJS. Lens integrated with self-aligned variable aperture using pneumatic actuation method. *Sens Actuators A*. 2010;159(1):105–110.
27. Doutel E, Viriato N, Carneiro J, Campos JB, Miranda JM. Geometrical effects in the hemodynamics of stenotic and non-stenotic left coronary arteries—numerical and in vitro approaches. *Int J Num Meth Biomed Eng*. 2019;35(8):e3207. doi:10.1002/cnm.3207
28. Usmani AY, Muralidhar K. Flow in an intracranial aneurysm model: effect of parent artery orientation. *J Visual*. 2018;21:795–818.
29. Kim S-J, Lee D-S, Kim I-G, et al. Evaluation of the biocompatibility of a coating material for an implantable bladder volume sensor. *Kaohsiung J Med Sci*. 2012;28(3):123–129.
30. Carta R, Jourand P, Hermans B, et al. Design and implementation of advanced systems in a flexible-stretchable technology for biomedical applications. *Sensors Actuators A*. 2009;156(1):79–87.
31. Alkilany AM, Alsotari S, Alkawareek MY, Abulateefeh SR. Facile hydrophobication of glutathione-protected gold nanoclusters and encapsulation into poly (lactide-co-glycolide) nanocarriers. *Scient Rep*. 2019;9(1):11098. doi:10.1038/s41598-019-47543-4
32. Chen Y-S, Kamat PV. Glutathione-capped gold nanoclusters as photosensitizers. Visible light-induced hydrogen generation in neutral water. *J Am Chem Soc*. 2014;136(16):6075–6082. doi:10.1021/ja5017365
33. Liu G, Feng D-Q, Hua D, Liu T, Qi G, Wang W. Fluorescence enhancement of terminal amine assembled on gold nanoclusters and its application to ratiometric lysine detection. *Langmuir*. 2017;33(51):14643–14648. doi:10.1021/acs.langmuir.7b02614
34. Fereja SL, Fang Z, Li P, et al. "Turn-off" sensing probe based on fluorescent gold nanoclusters for the sensitive detection of hemin. *Anal Bioanal Chem*. 2021;413:1639–1649. doi:10.1007/s00216-020-03126-1
35. Weng B, Zhang J, Shi Z-F, Tang Z, Zheng L-S, Xu Y-J. Improving the photostability of ultrasmall au clusters via a combined strategy of surface engineering and interfacial modification. *Langmuir*. 2019;35(17):5728–5736. doi:10.1021/acs.langmuir.9b00404
36. Wang Q, Wang R, Wang S, et al. Expansion and transmission dynamics of high risk carbapenem-resistant Klebsiella pneumoniae subclones in China: an epidemiological, spatial, genomic analysis. *Drug Resistance Updates*. 2024;74:101083.
37. Soni V, Khosla A, Singh P, et al. Current perspective in metal oxide based photocatalysts for virus disinfection: a review. *Journal of Environmental Management*. 2022;308:114617. doi:10.1016/j.jenvman.2022.114617
38. Iravani S. Nanophotocatalysts against viruses and antibiotic-resistant bacteria: recent advances. *Crit Rev Microbiol*. 2022;48(1):67–82.
39. Ge Y, Wang Q. Current research on fungi in chronic wounds. *Frontiers in Molecular Biosciences*. 2023;9:1057766. doi:10.3389/fmolb.2022.1057766
40. Oryan A, Alemzadeh E, Zarei M. Basic concepts, current evidence, and future potential for gene therapy in managing cutaneous wounds. *Biotechnol Lett*. 2019;41:889–898.
41. Raju NR, Silina E, Stupin V, Manturova N, Chidambaram SB. Multifunctional and smart wound dressings—a review on recent research advancements in skin regenerative medicine. *Pharmaceutics*. 2022;14(8):1574.